GFZ
Helmholtz-Zentrum
POTSDAM

Originally published as:

Risse, A., Trumbull, R. B., Coira, B., Kay, S. M., van den Bogaard, P. (2008): Ar-40/Ar-39 geochronology of mafic volcanism in the back-arc region of the southern Puna plateau, Argentina. - Journal of South American Earth Sciences, 26, 1, 1-15

DOI: 10.1016/j.jsames.2008.03.002

$^{40}Ar/^{39}Ar$ geochronology of mafic volcanism in the back-arc region of the southern Puna plateau, Argentina

Andrea Risse[1], Robert B. Trumbull[1*], Beatriz Coira[2], Suzanne M. Kay[3], Paul van den Bogaard[4]

[1] GeoForschungsZentrumPotsdam, Telegrafenberg, 14473 Potsdam, Germany

[2] Universidad Nacional de Jujuy, Instituto de Geología y Minería, SS de Jujuy, Argentina

[3] Cornell University, Dept of Earth and Atmospheric Sciences, Snee Hall, Ithaca, NY USA

[4] IFM-GEOMAR, Wischhofstr. 1-3, 24148 Kiel, Germany

Abstract

Late Cenozoic back-arc mafic volcanism in the southern Puna plateau of Argentina offers insights into the state of the mantle under the world's second largest continental plateau. Previous studies of the mafic magmas in this region proposed a scenario of mantle melting due to lithospheric delamination and/or steepening of the subducting slab. However, few of the centers have been precisely dated, which limits any geodynamic interpretation. We present results of laser incremental-heating $^{40}Ar/^{39}Ar$ dating of 22 back-arc centers in the southern Puna, with emphasis on the Salar de Antofalla region where volcanic activity was most intense. Three localities yielded ages between 7.3 and 7.0 Ma which, along with 2 previous 7 Ma ages, firmly establishes that back-arc activity began as early as late Miocene. Volcanism continued through the Pleistocene but the peak was in the early Pliocene. This result has important tectonic implications. If, as previously suggested, magma genesis is related to lithospheric delamination, this process was underway by the latest Miocene in the southern Puna. Furthermore, since the mafic back-arc volcanism is considered to mark a change in fault kinematics from compressional to transtensional, the new age constraints indicate that this change took place in the early Pliocene. The spatial and age distributions of the mafic centers indicate that magmatism began, and remained focussed in, a region between Salar de Antofalla and Cerro Galán. This concentration is probably structurally controlled as it corresponds to the intersection of the NW-SE striking Archibarca lineament zone and the sets of NNE-SSW faults that run parallel to the Salar de Antofalla basin.

Keywords: Central Andes, delamination, Ar-Ar geochronology, back-arc volcanism, Puna plateau

*Corresponding author: Fax, +49-331-2881474; email, bobby@gfz-potsdam.de

1 Introduction

The southern Puna plateau of Argentina is atypical of the Central Volcanic Zone (CVZ) in that there are relatively abundant late Miocene and younger mafic volcanic centers located behind the main volcanic arc. The importance of these back-arc mafic centers as indicators of the thermal and compositional state of the mantle source has long been recognized, and the overall features of their distribution and chemical characteristics are well established (Coira et al., 1982; Knox et al., 1989; Kay et al. 1994, 1997, 1999; Kraemer et al., 1999). The relative concentration of back-arc volcanism in the southern Puna features prominently in geodynamic arguments for late Cenozoic lithospheric delamination beneath this region as a consequence of shortening and crustal thickening (Kay et al., 1994; Whitman et al., 1996). Also, the back-arc volcanic activity is concentrated along faults and it has been suggested that magma ascent and eruption were favored by a shift in fault kinematics, from nearly-exclusive thrust faulting with NW-SE shortening through the Miocene, to an oblique-slip regime with a component of N-S extension in the late Pliocene (e.g., Coira et al., 1982; Marrett and Emerman, 1992; Marrett et al., 1994). However, two dates from 6 to 7 Ma were reported in the literature (Marrett et al., 1994; Kay et al., 1999; Kraemer et al., 1999) so clearly, the timing issue (onset and duration) needs further clarification before the volcanism can be related to tectonics and mantle processes (Kay et al., 1997). The purpose of this study was to improve the geochronological framework for back-arc mafic magmatism in the region with a program of Ar-Ar dating of well-characterized samples from the area between the Salar de Antofalla and the Cerro Galán caldera, where young mafic centers are most abundant.

2 Geological setting

Late Tertiary magmatism in the southern Puna is represented by three quite different volcanic associations (Coira et al., 1982; 1993): (i) andesitic-dacitic stratovolcanoes of early Miocene to Quaternary age in the main arc and middle Miocene to Pliocene ages in the back arc, (ii) Early Miocene to Pliocene dacitic-rhyolitic ignimbrites and lava domes that occur both in the main arc and back-arc region and (iii) small, late Miocene to Quaternary basic volcanic centers in the back arc which are of interest in this paper (Fig. 1). The oldest andesitic volcanoes recognized in the southern CVZ arc are the andesitic and basaltic andesitic León Muerto (20 Ma) and Cerro Colorado (19.5 Ma), both in the Western Cordillera of Chile. Miocene composite stratovolcanoes also extend east of the main arc, along NW-SE trending lineament zones (Fig. 1). Prominent

examples include the mid to upper Miocene Archibarca, Beltrán and Tebenquicho centers and the mid Miocene to Pliocene Antofalla volcanic complex (Coira and Pezzutti, 1976; Coira et al 1993; Kay et al. 1999; Kraemer et al. 1999, Richards et al., 2006), all of which are located near or along the Archibarca lineament in the northern Salar de Antofalla area (Fig. 1). Some of these composite volcanoes are remarkedly long lived (Tebenquicho: 14-6 Ma; Beltrán: 14-8 Ma, Antofalla: 11-2 Ma). Farther north, examples include the Rincon and Quevar centers along the Calama- Olacapato-El Toro lineament at about 24°S (Coira et al., 1993; Arnosio, 2002; Richards and Villeneuve, 2002; Matteini et al., 2002). Silicic magmatism in the southern Puna region (25-27°S) is mostly represented by ignimbrites. They cover about the same age interval as the arc activity and although most individual deposits are small in volume (<10 km^3) they occur over a wide area. In terms of their small size, generally rhyolitic composition and Sr-Nd isotope ratios like arc andesites, these ignimbrites are distinctly different from the huge dacitic ignimbrites with crustal signatures that predominate in the northern Puna and Altiplano (Coira et al., 1993; Siebel et al., 2001; Schnurr et al., 2007). A singular example of the latter type of ignimbrite in the southern Puna is the Cerro Galán caldera, which was active off and on since the latest Miocene but whose culminating eruption, with >1000 km^3, was at about 2 Ma (Sparks et al., 1985).

The mafic volcanic centers in the southern Puna back-arc region which are the subject of this paper consist of small, typically monogenetic to polygenetic cinder cones and lava flows. Many are calk-alkaline series basaltic andesites and andesites, with back-arc trace element affinities (Knox et al., 1989; Coira et al., 1993; Kay et al., 1994; Kraemer et al., 1999). It is worth pointing out that mafic back-arc volcanism is uncommon in the Central Volcanic Zone generally. Some mafic centers are known in northern Argentina, Bolivia and southern Peru, but these tend to be scattered, low-volume melts of K-rich calk-alkaline to shoshonitic compositions that erupted along faults and lineament zones (Déruelle, 1991; Sébrier and Soler, 1991; Davidson and de Silva, 1992). The southern Puna region studied here is anomalous for its relative abundance of young mafic centers, some of which have been shown by Kay et al. (1994) to possess intraplate geochemical characteristics (low Ba/Ta and low La/Ta ratios, among others). The other unusual volcanic feature, alluded to above, is the occurrence of the huge Cerro Galán caldera complex, which represents a major event of crustal melting as recently as 2 Ma (Sparks et al., 1985; Francis et al., 1989). Finally, a number of geophysical features in the southern Puna suggest unusually high mantle temperatures (strong seismic attenuation, low P- and S-wave velocities: see Whitman et al., 1992; Schurr et al., 2003;

Koulakov et al., 2006). The combination of intraplate mafic magmas, crustal melting and anomalous seismic properties of the mantle indicate that something happened to increase mantle melting, and one likely explanation is lithospheric delamination (Kay and Kay, 1993; Kay et al., 1994, 1999; Whitman et al., 1996).

The Tertiary tectonic history of the southern Central Andes is a central issue for interpreting the time-space distribution and characteristics of magmatism and its geodynamic controls and consequences. The literature on this subject is extensive and will not be reviewed here (Coira et al., 1993; Marrett et al., 1994; Kay et al., 1994, 1999; Allmendinger et al., 1997; Kraemer et al., 1999; Marrett and Strecker, 2000; Coutand et al., 2001; Oncken et al., 2006). One aspect of particular relevance to this study is the proposed change in deformation kinematics and style of faulting in the southern plateau region during the late Pliocene, from NW-SE shortening with vertical extension (thrust faults) to oblique-slip faults showing NE-SW or E-W shortening and N-S extension (Allmendinger, 1986;Marrett et al., 1994). The establishment of this new kinematic regime, which from fault scarp observations appears to continue into the present, has not been well constrained geochronologically (Marrett et al., 1994; Marrett and Strecker, 2000). This style of faulting is known to have started before the late Pliocene, based on ages of volcanic rocks along faults listed in Marrett et al. (1994) and discussed by Kay et al. (1999), and ages reported by Kraemer et al. (1999). Since many of the mafic centers in the southern Puna erupted along NNE-SSW trending oblique-slip faults (Fig. 2), their ages can have important implications with respect to the young tectonic history of the region.

3 Previous geochronology and new sampling strategy

A compilation of relevant results from radiometric studies reported in the literature is given in Table 1. Samples were included in this compilation only where the dating method and error estimate were provided and geographic coordinates or specific location were given. Excluded from the table are: (1) rocks more felsic than andesite (>63 wt.% SiO_2 if chemical data were given) and all tuffs, ash layers or ignimbrites regardless of composition; (2) rocks older than 10 Ma (to avoid confusion with the eastward-stepping Miocene arc volcanoes); (3) rocks whose age uncertainty was greater than 20% for ages> 2 Ma and greater than 50% for rocks <2Ma.

For the present study, we selected samples from 22 additional sites distributed throughout the study area. The samples were chosen to constrain the presumed oldest and youngest ages in the region, to augment existing age data in terms of geographic coverage, and to include all of the important geochemical types

present. Table 2 lists the locations and brief lithologic descriptions of the new samples. Chemical data (for data sources see Table 2) show that there are no true basalts in the sample suite based on the IUGS classification (LeMaitre et al., 1989). Instead, most samples classify as basaltic andesite to andesite, with a few exceptions being (basaltic) trachyandesites and one sample being dacitic (Fig. 3a). Based on their K_2O and SiO_2 concentrations, the rocks plot with the moderate to high-K series and none reach the shoshonite – banakite field (Fig. 3b). The great majority of samples selected for dating are fine grained, mildly porphyritic lavas, with phenocrysts comprising various proportions of olivine, clinopyroxene and plagioclase (± amphibole, ± orthopyroxene). The groundmass is generally microcrystalline and dominated by clinopyroxene, plagioclase and Fe-Ti oxides. Groundmass olivine is present in a few of the samples. Glass is a minor groundmass constituent (<5% to 20%) in many of the samples and in two examples (RAN2, SAF114), it makes up to 50% of the groundmass (Table 2). Signs of alteration are present but minor, and local in extent (iddingsite along cracks in olivine, hematitization of Fe-Ti oxide grains, devitrification of groundmass glass). Xenocrysts of quartz and/or plagioclase, rarely also pseudomorphs of amphibole (?), are not uncommon and many of the back-arc mafic lavas are vesicular, with local fillings of carbonate. Both the filled vesicles and xenocrysts are easily recognized and large enough (mm dimensions) to be avoided in the hand-picked groundmass separates that were prepared for dating (see below).

4. Analytic Methods

Samples for geochronology were crushed in a steel jaw crusher and sieved to isolate the 300 to 400 μm size fraction. Each sample was then carefully hand-picked under a binocular microscope to obtain homogeneous, clean, microcrystalline groundmass separates. These were then washed in distilled water in an ultrasonic bath and dried at 40°C. A 50 mg aliquot of each sample was wrapped in Cd foil and packed, along with flux monitor TCR-85G003 (Taylor Creek Rhyolite), in a revolving Al container for a 7-day irradiation in the FRG-1 reactor at GKSS Research Center Geesthacht. Laser step-heating and isotope analysis took place at the IFM-Geomar in Kiel (see Schwarz et al., 2005 for procedural details). A Spectra Physics 2040E-20 Ar-ion laser (488 and 514 nm) was used to heat between 5 and 15 mg of sample material. In this study, between 20 and 36 heating steps were carried out by sequentially increasing the laser power. Homogeneous heating for 60s at each step was achieved by rastering the defocussed laser beam across the sample surface. Isotopic analysis employed a MAP-216 noble gas mass spectrometer equipped with a Bauer-Signer-type ion source

and a Johnston electron multiplier. The gas extraction system was fitted to an ultraclean gas cleanup line of ca. 600 cc volume, with Zr-Al getters and LN_2 cold trap. Average extraction line blanks were determined at $4x10^{-14}$ cc STP at the masses 36 and 39, and $3x10^{-12}$ cc STP at mass 40. Mass discrimination was monitored using zero-age basaltic glass fused in air and pipette air samples and a correction factor of 1.008 per amu was applied. Correction factors for interfering neutron reactions on Ca and K were obtained from CaF_2 and K_2SO_4 grains that were irradiated with the samples. The $^{40}Ar/^{39}Ar$ ages were calculated relative to the flux monitor Taylor Creek Rhyolite (TCR) sanidine (27.92 Ma, Duffield and Dalrymple, 1990), which was calibrated against the standard SB-3 (162.9 Ma; Lanphere and Dalrymple, 2000). Uncertainties in the J value are estimated at ± 0.13% (1σ).

5 Results

Three types of age determinations were calculated for each sample: (1) a plateau age, evaluated from the apparent age spectrum of the 20 – 37 progressive heating steps according to the statistical criteria set out in McDougall and Harrison (1988); (2) an inverse isochron age, calculated from regression analysis of $^{36}Ar/^{40}Ar$ vs. $^{39}Ar/^{40}Ar$ data using the Isoplot 3.0 program of Ludwig (2003); and (3) an integrated or total gas release age. These three ages will coincide for the ideal case of perfect radiogenic Ar-retention, no ^{39}Ar recoil effects and no inherited Ar from contaminants. Discrepancies among the different ages are more common, and these may also give useful information. Overall, the step-heating experiments on matrix separates were successful in yielding intepretable ages in all but the youngest samples. In the presentation of results below, we describe the calculated ages of samples and give a preferred age where discordance or other problems were encountered. The full geochronology results and preferred ages are presented in the Appendix.

To aid in interpreting the Appendix and to avoid repetition in the descriptions below, step-heating results from three representative samples (Fig. 4) are described in some detail in order to illustrate the different types of Ar release behavior encountered in this study. In this and later sections, all quoted errors are at the 1σ level unless stated otherwise. The first example (SAF212) represents a simple spectrum and a near-perfect result, with concordant plateau, isochron and total-gas ages and an initial $^{40}Ar/^{36}Ar$ ratio indistinguishable from the atmospheric value of 295.5. Note that the uncertainty for isochron ages in this and all other cases is larger than for plateau ages because the former includes uncertainty in the initial $^{36}Ar/^{40}Ar$ ratio. For this sample, all temperature steps satisfy the criteria for inclusion in the plateau age (McDougall

and Harrison, 1988) but the low-temperature steps are dominated by atmospheric Ar and yielded lower Ca/K ratio values than the rest, presumably reflecting a minor contribution from secondary K-poor phases. The second example, from sample SAF214, illustrates a less ideal, but more common case of a step-heating experiment where the Ar release spectrum is complex and a plateau age (2.43 ± 0.07 Ma) is defined by intermediate temperature steps (in this case, 11 consecutive steps comprising 87% of the ^{39}Ar released. The higher-temperature steps yield older apparent ages and the total-gas age for this sample (2.6 ± 0.1 Ma) is discordant and high. The fact that these high-T steps also yielded high Ca/K ratios and low radiogenic ^{40}Ar* compared with the "plateau steps" suggests that a relatively K-poor material contributed to the Ar release at high temperature. A likely explanation for this behavior is Ar degassing from phenocrystic and/or groundmass pyroxenes and plagioclase which, as witnessed by the high apparent age, contained some excess Ar. Note that the relatively high uncertainty of individual apparent age for the lowest-temperature step and for steps 13 to 14 technically permit them to be included in the plateau (concordant ages within 2σ for adjacent steps), but our preferred age for this sample is based on the restricted plateau comprising steps 2 to 12. The isotope correlation diagram for sample SAF214 shows considerable scatter but regression of the 11 plateau-defining steps results in a statistically acceptable isochron age of 2.3 ± 0.1 Ma (MSWD = 1.4), concordant with the plateau age. The initial ^{40}Ar/^{36}Ar ratio is 297 ± 1, or slightly above the atmospheric value. Regressing all steps together gives an even higher initial ratio (298.3), indicating some contamination from a non atmospheric Ar component. The last example shown in Fig. 4 illustrates some of the difficulty interpreting the age of the very young samples (RM810). The Ar release spectrum is complex, with a rise in apparent age in high-temperature steps as seen in the previous example, which results in a higher total-gas age than the plateau or isochron ages. Typical for this and other samples with Quaternary apparent ages is the low to very low percentage of radiogenic ^{40}Ar* in the gas release, which contributes to disproportionately large uncertainties in apparent ages compared with the older samples. Because of the high individual age uncertainties, more of the heating steps fall within the plateau criteria; indeed for sample RM810, this means that all steps can be included in the plateau calculation. However, the Ar release spectrum is obviously not homogeneous and the total gas age is discordantly high. Thus in this case and others like it, our preferred age is calculated from a restricted plateau. For RM810 the restricted plateau comprises the first 7 steps (68% ^{39}Ar released). The plateau and restricted plateau ages agree within error large (0.79 vs. 0.8, each ± 0.1 Ma) but the MSWD value of the latter is much improved (0.2 vs. 1.5 for the total plateau, see Appendix). The

isochron analysis for this sample gives a rather imprecise but concordant age of 0.7 ± 0.2 Ma, MSWD 0.2) for the restricted plateau steps and an atmospheric initial ratio of 296 ± 2.2.

The rest of the samples analyzed show features similar to those illustrated in Fig. 4 and they will not be discussed in detail individually except where necessary to explain the preferred age assignment. For all but a very few of the youngest samples, the step-heating experiments allow a straightforward age interpretation and the following discussion is therefore limited to mention of the calculated ages and their degree of concordance for each sample, the preferred age assignment and an illustration of the Ar release spectra (Fig. 5). To structure the presentation somewhat, results are discussed below in groups of decreasing age.

5.1 Late Miocene to early Pliocene centers

The oldest ages obtained for back-arc minor centers in this study are from three samples (SAF66, 8373 and 8371) located east of the Salar de Antofalla. All yielded ages of about 7 Ma. Sample SAF66 is a basaltic andesite from the lower lava flow at La Alumbrera, located ca. 7 km south of Antofagasta de la Sierra. The sample yielded concordant plateau (7.34 ± 0.04 Ma, 14 steps) and isochron ages (7.30 ± 0.05 Ma), and a slightly older total-gas age of 7.64 ± 0.05 Ma. Sample 8373, from southeast of Antofagasta de la Sierra is a dacitic lava, which yielded a plateau age of 6.98 ± 0.06 Ma (70%, with ^{39}Ar yield) that is concordant with its isochron age (7.0 ± 0.2 Ma, atmospheric 295.1 ± 1.7 initial ^{40}Ar/^{36}Ar ratio) and its total-gas age of 6.80±0.08 Ma. The third sample in this group (8371 is an andesite lava flows from a locality 5 km NW of Antofagasta de la Sierra. It also yielded concordant plateau and isochron ages, with 7.13 ± 0.08 Ma (87% ^{39}Ar yield) and 6.9 ± 0.3 Ma, respectively. The initial ^{40}Ar/^{36}Ar ratio for this sample is 296.3 ± 1.1, indistinguishable from the atmospheric ratio.

Three samples from the northern part of the Salar de Antofalla west of Cerro Beltrán (RM568, SAF31, SAF24) yielded ages of 4-5 Ma. Sample RM568 is a basaltic andesite from a lava flow at Vegas Colorado. The apparent age spectrum for this sample yielded a well-defined plateau (4.6 ± 0.2 Ma, 54% ^{39}Ar released), and a concordant total-gas age of 5.1 ± 0.2 Ma). Isochron analysis for this sample yielded a concordant but rather imprecise age of 4.9 ± 1.4 Ma. The uncertainty is due to the narrow spread of ^{36}Ar/^{40}Ar values near the X-axis. The initial ^{40}Ar/^{36}Ar ratio is significantly higher than the atmospheric value, indicating some contamination by a non-atmospheric component. Sample SAF31 is a cpx-opx-plag andesite with amphibole

from the peninsula region in the Salar de Antofalla. The age results for this sample are also concordant, with a plateau age of 4.82 ± 0.05 Ma (65% ^{39}Ar yield), total-gas age of 4.92 ± 0.05 Ma and an isochron age of 4.9 ± 0.12 Ma, with atmospheric initial ^{40}Ar/^{36}Ar ratio. Finally, sample SAF24, an olivine-bearing basaltic trachyandesite from the Quebrada del Diablo, gave a rather poorly-defined plateau age (4.3 ± 0.2 Ma, only 54% ^{39}Ar released) and a concordant but imprecise isochron age (3.7 ± 1.4 Ma) with a near-atmospheric initial ^{40}Ar/^{36}Ar ratio. The total-gas age of this sample is significantly older (6.1 ± 0.2 Ma) due to the rise in apparent age (inherited Ar) for the high-temperature steps. Also in this age range are two samples from south of Antofagasta de la Sierra, 8379 from Jote and 8382 from east of La Alumbrera. The Jote sample 8379, a basaltic andesite, gave a rather disturbed Ar release spectrum (Fig. 5) and a plateau age of 3.5 ± 0.1 Ma (66% ^{39}Ar released) which is discordant to the total-fusion age of 4.0 ± 0.1 Ma. The isochron age of this sample is 4.5 ± 0.3 Ma and its initial ^{40}Ar/^{36}Ar ratio is 294.9 ± 0.6. Results for the andesite flow sampled near la Alumbrera (8382) show a near-perfect behavior, with a plateau defined by 99% ^{39}Ar release yielding an age of 4.2 ± 0.2 Ma and identical isochron age with an atmospheric initial ^{40}Ar/^{36}Ar ratio of 296.4 ± 2.

Finally, sample SAF212 from a micro-to cryptocrystalline silicic andesite southwest of Salar de Hombre Muerto gave an early Pliocene age and provides a textbook example of near-perfect Ar-Ar result (see Fig. 4). All 20 heating steps for this sample meet the plateau criteria and the resulting age is 4.62 ± 0.04 Ma. Both the total-gas and isochron age results are concordant with the plateau age (4.58 ± 0.7 Ma and 4.61 ± 0.05 Ma, respectively), and the initial ^{40}Ar/^{36}Ar ratio is indistinguishable from the atmospheric value.

5.2 Late Pliocene centers

The next-younger age group of samples is late Pliocene (3.2 - 2.4 Ma) in age. This group is represented by an upper flow from the Jote center (SAF218) and three samples from north of Antofagasta de la Sierra (SAF202, SAF200, SAF207). Sample SAF218 is an olivine-phyric basaltic andesite which gave a plateau age of 3.2 ± 0.2 Ma (53% ^{39}Ar release) and concordant total-gas age of 2.9 ± 0.2 Ma. The isochron analysis gave poor results. Regression of all steps yield a discordantly young age of 1.6 ± 0.8 Ma with a poor MSWD = 3.4 and high initial ratio of 299.2 suggesting non-atmospheric contamination. If only the plateau-forming steps are used, the isochron age is even negative. Samples SAF 202 and SAF 200 represent closely adjacent flows of ol-cpx-andesite and basaltic andesite flows, respectively, from the area of Los Nacimientos about 20 km north of Antofagasta de la Sierra. Both yielded late Pliocene ages. The data from SAF 202

define a plateau age of 2.8 ± 0.2 Ma (82% ^{39}Ar yield) and concordant isochron age (2.8 ± 0.3 Ma). The total-gas age for this sample is slightly older, at 3.3 ± 0.2 Ma. Fully concordant age results were obtained for sample SAF200, with a plateau age of 2.50 ± 0.06 Ma (62% ^{39}Ar yield) and isochron age of 2.5 ± 0.1 Ma, and total-gas age of 2.61 ± 0.06 Ma. Samples SAF207 and 8367 represent olivine-basaltic andesite lavas from Cerro Chinina, ca. 25 km north of Antofagasta. Their ages are very similar to those of the older flows from Los Nacimientos. The plateau age for SAF207 is 2.4 ± 0.1 Ma (73% ^{39}Ar release) and both the isochron age (2.8 ± 0.2 Ma) and total-gas age for this sample (2.5 ± 0.1 Ma) are concordant within error. Geologic support for the 2.5 Ma age comes from the fact that the lava flow sampled at this outcrop is overlain by an outflow sheet of the Galán ignimbrite, whose age according to Sparks et al. (1985) is 2.03 ± 0.07 Ma (Rb-Sr internal isochron) or 2.5 ± 0.1 (K-Ar, biotite). Sample 8367 gave a plateau age of 2.48 ± 0.06 Ma (58% ^{39}Ar yield), with a concordant isochron age (2.43 ± 0.09 Ma) and a slightly higher total-gas of 2.88 ± 0.06, showing influence of the high-temperature steps (Fig. 5). Finally, sample SAF214 from a basaltic andesite flow near the Tincalayu borax mine on the north edge of Salar de Hombre Muerto, yielded a well-defined late Pliocene plateau age of 2.43 ± 0.07 Ma (87% ^{39}Ar released), which agrees within uncertainty with the isochron age (2.3 ± 0.1 Ma). As discussed in more detail above (see Fig. 4), the high-temperature steps for this sample gave higher apparent ages and the total-gas age for this sample is 2.6 ± 0.1 Ma.

5.3 Quaternary centers

A number of samples yielded Quaternary ages. Many of the Ar-release spectra are not easy to interpret for age significance. A representative example of this group (RM810) was described in detail above (see Fig. 4). This sample is a basaltic andesite flow from the Farallon Catal locality within the Salar de Hombre Muerto (Fig. 2). The preferred age is 0.8 ± 0.1 Ma based on a restricted plateau (68% ^{39}Ar released). The high temperature steps yield elevated apparent ages. but their contribution to the total-gas age is not enough to raise it significantly (0.8 ± 0.1). The isochron age of this sample, calculated from the plateau-defining steps, is concordant at 0.7 ± 0.2 Ma. A sample of basaltic andesite from the Los Nacimientos area (8368) was analyzed with only 5 heating steps so we report the total-gas age (1.5 ±0.1 Ma) and the concordant isochron age of 1.5 ± 0.8 Ma with an initial ^{40}Ar/^{36}Ar ratio of 296 ± 4 (Fig. 5, Appendix). Two samples from the southwestern corner of the study area also gave Quaternary ages. Sample CO-99 is a basaltic trachyandesite from the southern end of Salar de Antofalla. The Ar release spectrum defined a good plateau age despite the

youth of this sample, with 0.6 ± 0.1 Ma (59% ^{39}Ar released). The total-gas age of the sample is concordant within uncertainty (0.5 ± 0.1 Ma) whereas isochron analysis yielded a slightly older age of 0.8 ± 0.1 Ma, with a near-atmospheric initial ratio. The Ar-Ar results from the other southern salar sample, SAF76 from the Laguna Purulla area east of the salar, are more difficult to interpret. Two aliquots of this sample were analyzed. The total-gas age of both are the same (0.46 Ma) but the Ar release spectra indicate a complex degassing behavior only one of the two experiments permit definition of a plateau ages (0.8 ± 0.1 Ma, 58.5% ^{39}Ar released) which, unusually, is significantly higher than the total-gas ages. The isochron results for this sample fail to define an age significantly different from zero. Finally, three samples from localities south and west of Antofagasta de la Sierra (SAF65, SAF71, RAN2) yielded Quaternary apparent ages, but because of the very low abundance of radiogenic ^{40}Ar and relatively high contamination from atmospheric Ar, the age estimates have large errors and considerable discordance. Two aliquots of sample SAF71, a basaltic trachyandesite from Carachi Pampa center, were run (SAF71-MX and SAF71-MX2). The second of these yielded an acceptable plateau age (0.75 ± 0.08 Ma, 66% ^{39}Ar released). The total-gas age (0.73 ± 0.08 Ma) is concordant with the plateau but the isochron analysis for this sample failed to return a non-zero age. Sample SAF65, a basaltic andesite from La Laguna, gave a poorly-defined plateau age, which is dominated by high temperature steps (0.34 ± 0.06 Ma, 45% ^{39}Ar released) and considered to be a mixed age representing matrix degassing with a older contribution from phenocrysts. For this sample, neither the total-gas nor isochron age significantly different from zero. Finally, for sample RAN2, a basaltic andesite from La Falda, all three estimates returned zero-age values and we assign the sample an estimate of <0.1 Ma. The sampled flow is morphologically young and free of apparent weathering or alteration, in agreement with this result.

6 Discussion

From the 22 new samples dated in this study, all but two of the youngest ones yielded reasonable to excellent plateau ages and concordant isochron ages. The range of the resulting ages is 7.3 to 0.3 Ma and younger. We interpret these as representing the time of eruption rather than not cooling ages because of the small volumes of the dated centers and their fine-grained to glassy textures. For the same reasons, and noting the relatively low and uniform degree of geochemical fractionation of the mafic centers, long periods of magma storage in the crust before eruption are unlikely (see also Francis et al. 1989; Davidson and de Silva, 1992), and therefore the dates obtained are relevant for the age of magma formation.

Several earlier studies that addressed the tectonic implications of the back-arc mafic magmatism in the region considered it to be Pliocene and younger (Allmendinger, 1986; Coira et al., 1993; Marrett et al., 1994; Kay et al., 1994), and this age continues to be quoted (e.g. Gregory-Wodzicki, 2000; Beck and Zandt, 2002) despite mention of considerably older ages for the onset of back-arc activity by Kay et al. (1999) and Kraemer et al. (1999). The latter study reported late Miocene ages for two samples (Table 1) and our results document an additional 3 sites with ages of 7 Ma. The onset of mafic volcanism in the southern Puna back-arc region is therefore firmly established to be at least late Miocene in age. The conception that back-arc volcanism in the southern Puna is a young phenomenon results partly from the good preservation of mafic centers and lava flows in the high, arid plateau and their morphologically young appearance on satellite images (Fig. 6). The reduced ability to estimate eruption ages from remote imaging in hyperarid regions like the southern Puna has wider implications for assessing potentially active volcanic fields in remote areas. The use of volcanic morphology as an age proxy clearly needs "calibration" for specific climatic conditions and lithologic makeup.

6.1 Time-space distribution of back-arc volcanism

Figure 7 displays a stacked frequency histogram combining the 22 new ^{40}Ar-^{39}Ar results from this study with 21 previous dates of back-arc centers compiled on Table 1. Although 43 localities have now been dated, this is only a fraction of the mafic cones and fissure flows present in the study area (compare Fig. 2). Nevertheless, the results are sufficient to demonstrate that back-arc mafic magmatism began as early as 7.3 Ma in the region and that there is a peak of activity at 6 to 4 Ma, which includes 19 of the 43 ages. Kay et al. (1999) and Kraemer et al. (1999) suggested that the main phase of back-arc activity was early Pliocene based on data then available, and this is confirmed by the new data. Volcanic activity drops off after 4 Ma and continues with some fluctuations through the Pleistocene. The apparent pulses of activity at 3-2 Ma and 1-0 Ma implied by Figure 7 may not be significant because of the small number of samples. The main conclusion from this compilation is that the back-arc mafic volcanism in the southern Puna, which had once been considered as late Pliocene and younger, began in fact at least by the late Miocene and appears to have reached a maximum in the early Pliocene (6-4 Ma).

It is worth comparing the age distribution of the relatively small-volume mafic volcanism in the back-arc with that of the other volcanic associations in the region. The late Miocene/early Pliocene onset and peak

of mafic volcanism coincides with the waning activity of the large composite centers in the back arc (Beltran, Archibarca, Antofalla and Tebenquicho volcanoes), which represent eastward outliers of the main arc along the Archibarca lineament zone (Fig. 2). The comparison with activity in the adjacent segment of the main arc (25° to 27°S and 68° to 69°W) is shown in the shaded histogram at the top of Figure 7 based on the data compilation by Trumbull et al. (2006) . Because we are interested in the relative timing of mantle melting in the two regions, data for silicic units and ignimbrites are not included in the compilation. The histogram of main arc activity (n=144) shows a broad maximum during the late Miocene time when mafic volcanism in the back arc became established, but there is no correlation in detail between the two regions and in particular, nothing in the main arc record corresponds with the peak in back-arc activity at 6-4 Ma. This comparison suggests that the rates of magmatism in the back arc and main arc regions varied independently of each other and were not related. On the other hand, the back-arc age variations do show a correlation with the timing of major silicic ignimbrite eruptions from the Cerro Galán complex (arrows on Fig. 7, based on the study of Sparks et al., 1985). The two older ignimbrite units from Galán, Merihuaca (6.3 to 5.1 Ma) and Real Grande (4.8 to 5.1 Ma), are contemporaneous with the peak of mafic magmatism, whereas the main caldera-forming event which produced the >1000 km^3 Galán ignimbrite took place at about 2 Ma (Sparks et al., 1985). The geochemical and radiogenic isotope composition of all three Galán ignimbrites indicate a dominantly crustal origin for the magmas produced (Francis et al., 1989), and it is likely that both the crustal melting and the eruption of mafic lavas in the back-arc region are both related to the same cause: an enhanced heat input from the mantle (Kay et al., 1994; 1999; Coira et al., 1993). It can be expected that theestablishment of the large crustal magma system(s) associated with the Galán ignimbrites affected the local stress field and the rheologic behavior of the upper crust. (e.g., de Silva et al., 2006), and this could be reflected in patterns of timing, localization and character of the mafic lavas.

The geographic distribution of all dated mafic back-arc centers is shown in Figure 8 with symbols coded for the age ranges 0-2 Ma, 2-4 Ma, 4-6 Ma and 6-8 Ma. Based on the present sample coverage, it appears that the older centers (>4 Ma) are concentrated in an area east of Salar de Antofalla between 25°30'S and 26°15'S whereas the late Pliocene and younger centers are more uniformly distributed throughout the study area. This age-distribution pattern may need revision as more dates become available, but the fact that there is a concentration of activity in the area of initial volcanism between Antofalla Salar and Galán caldera is confirmed by geologic maps and satellite images (Fig. 2). The reason for this concentration of volcanism is

speculative. Clearly, one controlling factor is the location of significant melting in the back-arc mantle, and evidence for high mantle temperatures beneath the Antofalla-Galán region today was shown by P- and S-wave tomography sections across the arc and back-arc at 25.5°S by Heit (2006). However, considering that magmas must penetrate and then traverse the approximately 60 km-thick crust of the southern Puna (Woelbern et al., 2006; Heit, 2006), it is also likely that the spatial distribution of volcanism is also influenced by structures favorable for magma ascent. An association of young mafic cones and fissure flows with NNE-trending faults in the southern Puna has long been recognized (e.g., Hörmann et al., 1973; Coira and Pezzutti, 1976; Allmendinger, 1986; Coira et al., 1993; Marrett et al., 1994; Marrett and Strecker, 2000). However, the abundance of faults alone does not explain the regional concentration of mafic centers and we consider it more likely that magma ascent and emplacement were influenced by the regional NW-SE striking Archibarca lineament zone and its intersection with NNE-SSW-trending faults bounding the Salar de Antofalla basin and uplifted basement blocks. The Archibarca lineament zone has clearly played an important role for magma emplacement since the mid-Miocene (Coira et al., 1993; Chernikoff et al., 2002; Richards et al., 2006), like the Calama-Olacapato-Toro lineament farther north (Matteini et al., 2002; Petrinovic et al., 2006). It is significant that a second, smaller cluster of mafic centers occurs at the intersection of the Culampaja lineament zone and the southern end of the Salar de Antofalla structure (see Fig. 2).

7 Conclusions

The results of laser step-heating $^{40}Ar/^{39}Ar$ dating of 22 andesitic to basaltic andesite volcanic centers in the back-arc region around the Salar de Antofalla, southern Puna plateau, document a total range of 7.3 to 0.3 Ma and younger. Combining the new and existing results (n = 42), the onset of back-arc mafic activity is firmly established at least as early as 7 Ma. The data also demonstrate a peak in volcanism at 6-4 Ma, after which activity continued at a lower level, with fluctuations, through the Pleistocene.

The age distribution of mafic centers in the back arc shows no correlation with variations in activity of the main volcanic arc, indicating that controls on mantle melting in the two regions were independent of each other. However, there is a correspondence in time between the peak of back-arc mafic volcanism and the first major eruptions of large-volume felsic ignimbrites from the nearby Cerro Galán caldera complex. The Galán magmas are largely crustal derived and it is likely that the increased vigor of back-arc magmatism and the

production of extensive crustal melts are both manisfestations of enhanced melting in the mantle. The cause of this melting anomaly has been postulated to involve an influx of asthenospheric mantle related to delamination of the lower crust and lithospheric mantle following crustal thickening, or to a steepening/rollback of the subducting plate (e.g., Coira et al. 1993; Kay et al., 1994, 1999). Whatever factor of combination of factors, the geochronology results indicate that the process was under way by 7 Ma. Many of the back-arc volcanic centers occur along reactivated high-angle reverse faults and their eruption was proposed to herald a change in regional stress conditions in the southern Puna plateau. Studies by Allmendinger (1986), Marrett et al. (1994) and Marrett and Strecker (2000) proposed that this kinematic change in the late Pliocene based on ages then available. The peak of back-activity at 6-4 Ma implies that the transition in stress conditions occurred considerably earlier, at least in the Salar de Antofalla region.

Acknowledgements

This work was carried out as part of the lead author's PhD study and was supported by the German DFG within the SFB-267 collaborative research center "Deformation Processes in the Andes". We thank Pablo Caffe, Constantino Mpodozis, Richard Allmendinger and Randy Marrett for their participation in collecting some of the samples that were dated in this study and for sharing their knowledge of and enthusiasm for Andean geology. AR acknowledges Jose Viramonte for a stimulating introduction to Puna geology during his 2002 volcanology field course, and for help in collecting a key sample. Peter Pilz, Stefan Sobolev, Manfred Strecker and many other colleagues in the SFB-267 group are thanked for numerous discussions on Andean geology and geophysics. SK acknowledges support from US NSF grant 00-87515.

References

Adelmann, D., 2001. Känozoische Beckenentwicklung des zentralandinen Puna-Plateaus (NW Argentinien) – Das Gebiet um den Salar de Antofalla und ein Vergleich zur nördlichen Puna. PhD Thesis, Free University of Berlin. Berliner Geowissenschafliche Abhandlungen Reihe A, 210.

Allmendinger, R.W., Jordan, T.E., Kay, S.M., Isacks, B.L., 1997. The evolution of the Altiplano-Puna of the Central Andes. Annual Reviews of Earth and Planetary Sciences, 25: 139-174.

Allmendinger, R.W., 1986. Tectonic development, southeastern border of the Puna Plateau, northwestern Argentine Andes, Geological Society of America Bulletin, 97: 1070-1082..

Arnosio, J.M., 2002. Volcanismo, geoquimica y petrología del volcan Chimpa (24°S, 66°W), Provincia de Salta, Republica Argentina. Ph.D. Thesis, Universidad Nacional de Salta, Argentina. 139 pp.

Beck, S.L., Zandt, G., 2002. The nature of orogenic crust in the central Andes. Journal of Geophyical Research, 107: 10.1029/2000JB000124.

Chernicoff, C.J., Richards, J.P., Zappettini, E.O., 2002. Crustal lineament control on magmatism and mineralization in northwestern Argentina: geological, geophysical, and remote sensing evidence. Ore Geol. Rev., 21: 127-155.

Coira, B., Kay, S.M., 1993. Implications of Quaternary volcanism at Cerro Tuzgle for crustal and mantle evolution of the Puna Plateau, Central Andes, Argentina. Contrib. Mineral. Petrol., 113: 40-56.

Coira B., Pezzutti, N., 1976. Vulcanismo cenozoico en el ámbito de Puna Catamarqueña. Revista Asociación Geológica Argentina XXXI (1), 33-52.

Coira, B., Davidson J, Mpodozis, C., Ramos, V., 1982. Tectonic and magmatic evolution of the Andes of Northern Argentina and Chile. Earth Science Reviews, 18: 302-332.

Coira, B., Kay, S.M., Viramonte, J.G., 1993. Upper Cenozoic magmatic evolution of the Argentine Puna - A model for changing subduction geometry. International Geology Review, 35: 677-720.

Coutand, I., Cobbold, P.R., de Urreiztieta, M., Gautier, P., Chauvin, A., Gapais, D., Rosselo, E.A. and López-Gamundi, O. (2001) Style and history of Andean deformation, Puna Plateau, northwestern Argentina, Tectonics, 20: 210-234.

Davidson, J.P., de Silva, S.L., 1992. Volcanic rocks from the Bolivian Altiplano: Insights into crustal structure, contamination, and magma genesis in the central Andes, Geology, 20: 1127-1130.

Déruelle, B., 1991, Petrology of Quaternary shoshonitic lavas of northwestern Argentina. Geol. Soc. America Sp.Paper 265: 201-216.

de Silva, S.L., Francis, P., 1991. Volcanoes of the Central Andes.Springer-Verlag, New York, 216 pp.

de Silva, S.L., Zandt, G., Trumbull, R.B., Viramonte J.G., Salas, G., Jimenez, M., 2006. Large-scale silicic volcanism in the Central Andes – a tectonomagmatic perspective. In: Troise, C., deNatale, G., Kilburn, C.R.J. (Eds) Mechanisms of Activity and Unrest at Large Calderas. Geol. Soc. London Special Publication 269: 47-63.

Duffield, W.A., Dalrymple,G.B., 1990. The Taylor Creek rhyolite of New Mexico: a rapidly emplaced field of domes and lava flows. Bull. Volcanology, 52: 475-478.

Francis, P.W., Sparks, R.S.J., Hawkesworth, C.J., Thorpe, R.S., Pyle, D.M., Tait, S.R., Mantovani, M.S., McDermott, F., 1989. Petrology and geochemistry of volcanic rocks of the Cerro Galan caldera, northwest Argentina. Geological Magazine, 126: 515-547.

Gregory-Wodzicki, K.M., 2000. Uplift hisory of the Central and Northern Andes: a review. Geological Society of America Bulletin, 112: 1091-1105.

Heit, B.S. (2006) Teleseismic tomographic images of the Central Andes at 21°S and 25.5°S: an inside look at the Altiplano and Puna plateaus. GeoForschungsZentrum Potsdam Scientific Technical Report STR06/05, 139 pp.

Hörmann, K.P., Pichler, K.H., Zeil, W., 1973. New data on the young volcanism in the Puna of NW-Argentina. Geologische Runschau, 62: 397-428.

Kay, R.W., Kay, S.M., 1993. Delamination and delamination magmatism. Tectonophysics, 219: 177-189.

Kay, S.M., Coira, B., Viramonte, J.G., 1994. Young mafic backarc volcanic rocks as indicators of continental lithospheric delamination beneath the Argentine Puna Plateau, Central Andes. Journal of Geophysical Research, 99: 24323-24339.

Kay S.M., Coira, B., Mpodozis, C., 1997. Southern Central Volcanic zone arc and backarc mafic magmas: signals of andean lithospheric processes (27º- 25º S). VIII Congreso Geológico Chileno. Actas III:1656-1661.

Kay, S.M., Mpodozis, C., Coira, B., 1999. Neogene magmatism, tectonism, and mineral deposits of the Central Andes (22ºS to 33ºS). In: B. Skinner (Ed.). Geology and ore deposits of the central Andes.

Knox, W.J.Jr., Kay, S.M., Coira, B., 1989. Geochemical evidence on the origin of Quaternary basaltic andesites of the Puna, northwestern Argentina. Rev. Asoc. Geol. Argentina, 44: 194-206.

Koulakov, I., Sobolev, S.V., Asch, G. 2006. P- and S-velocity images of the lithosphere-asthenosphere system in the Central Andes from local-source tomographic inversion, Geophys. J. Int., 167: 106-126.

Kraemer, B. Adelmann, D., Alten, M., Schnurr, W., Erpenstein, K., Kiefer, E., van den Bogaard, P., Görler, K., 1999. Incorporation of the Paleogene foreland into the Neogene Puna Plateau; the Salar de Antofalla area, NW Argentina. Journal of South American Earth Sciences, 12: 157-182.

Lanphere, M.A., Dalrymple, G.B., 2000. First-principles calibration of ^{38}Ar tracers: implications for ages of ^{40}Ar/^{39}Ar fluence monitors. U.S. Geol.Surv. Prof. Paper 1621, 10 pp.

Le Maitre, R.W., Bateman, P., Dudek, A., Keller, J., Lameyre Le Bas, M.J., Sabine, P.A., Schmid, R., Sorensen, H., Streckeisen, A., Woolley, A.R., Zanettin, B. (1989) A classification of igneous rocks and glossary of terms. Blackwell, Oxford.

Ludwig, K.R., 2003, Isoplot 3.00 A geochronological toolkit for Microsoft Excel, Berkeley Geochronology Center Special Publication No.4

Marrett, R.A., Strecker, M.R., 2000. Response of intracontinental deformation in the central Andes to late Cenozoic reorganization of South American plate motions. Tectonics, 19: 452-467.

Marrett, R.A., Allmendinger, R.W., Alonso, R.N., Drake, R.E., 1994. Late Cenozoic tectonic evolution of the Puna Plateau and adjacent foreland, northwestern Argentine Andes. Journal of South American Earth Sciences, 7: 179-207.

Marrett, R., Emermann, S. H. 1992. The relations between faulting and mafic magmatism in the Altiplano-Puna plateau (central Andes), Earth and Planetary Science Letters, 112: 53-59.

Matteini, M., Mazzuoli, R., Omarini, R., Cas, R., Maas, R., 2002. The geochemical variations of the upper Cenozoic volcanism along the Calama-Olacapato-El Toro transversal fault system in central Andes (24°S): petrogenetic and geodynamic implications. Tectonophysics, 345: 211-227.

McDougall, I., Harrison, T.M., 1988. Geochronology and Thermochronology by the ^{40}Ar/^{39}Ar Method. Oxford University Press, London/New York, 212 pp.

Middlemost, E.A.K., 1980. A contributionto the nomeclature and classification o f volcanic rocks. Geological Magazine, 117: 51-57.

Oncken, O., Hindle, D., Kley, J., Elger, K., Victor, P., 2006. Deformation of the Central Andean upper plate system – facts, fiction, and constraints for plateau models. In: Oncken, O. et al. (eds) The Andes – from Top to Bottom. Frontiers in Earth Sciences, 1. Springer-Verlag, Heidelberg, Berlin, New York (in press)

Ramos, V.A., Cegarra, M., Cristallini, E., 1996. Cenozoic tectonics of the High Andes of west-central Argentina (30-36°S latitude). Tectonophysics, 259: 185-200.

Richards, P.R., Ullrich, T., Kerrich, R., 2006. The Late Miocene-Quaternary Antofalla volcanic complex, southern Puna, NW Argentina: Protracted history, diverse petrology, and economic potential, Journal of volcanology and Geothermal Research, 152: 197-239.

Richards, J.P., Villeneuve, M., 2002. Characteristics of the late Cenozoic volcanism along the Archibarca lineament from Cerro Llullaillaco to Corrida de Cori, northwest Argentina. Journal of Volcanology and Geothermal Research, 116: 161-200.

Salfity, J.A., 1985. Lineamentos transversales al rumbo andino en el Noroeste Argentino. Actas del 4. Congreso Geologico Chileno, 2: A119-A127.

Schnurr, W.B.W., Risse, A., Trumbull, R.B., Munier, K., 2006. Digital Geological Map of the Southern and Central Puna Plateau, NW Argentina. In: Oncken, O. et al. (eds) The Andes – Active Subduction Orogeny. Frontiers in Earth Sciences, 1. Springer-Verlag, Berlin, Heidelberg, New York., p. 563-564.

Schnurr,W.B.W., 2001. Zur Geochemie und Genese neogener und quartärer felsischer Vulkanite in den südlichen Zentralanden (25°-27° S und 67°-69°W) Berliner Geowissenschafliche Abhandlungen Reihe A, 211, 152 pp.

Schnurr, W.B.W., Trumbull, R.B., Clavero, J., Hahne, K., Siebel, W., Gardeweg, M., 2007. Twenty-five million years of silicic volcanism in the southern Central Volcanic Zone of the Andes: geochemistry and magma genesis of ignimbrites from 25-27°S, 67-72°W. Journal of Volcanology and Geothermal Research (in press)

Schurr, B., Asch, G., Rietbrock, A., Trumbull, R. and Haberland, C., 2003. Complex patterns of fluid and melt transport in the central Andean subduction zone revealed by attenuation tomography, Earth and Planetary Science Letters, 215: 105-119.

Schwarz, S., Klügel, A., van den Bogaard, P., Geldmacher, J., 2005. Internal structure and evolution of a volcanic rift system in the eastern North Atlantic: the Desertas rift zone, Madeira archipelago. Journal of Volcanology and Geothermal Research, 141: 123-155.

Sébrier, M., Soler, P., 1991. Tectonics and Magmatism in the Peruvian Andes from late Oligocene Time to the Present. In: Harmon, R.S. and Rapela, C.W. (eds.) Andean Magmatism and its Tectonic Setting. GSA Special Paper 265: 259-278.

Siebel, W., Schnurr, W.B.W., Hahne, K., Kraemer, B., Trumbull, R.B., van den Bogaard, P. and Emmermann, R. 2001. Geochemistry and isotope systematics of small- to medium volume Neogene-Quarternar ignimbrites in the southern central Andes: evidence for derivation from andesitic magma sources, Chemical Geology, 171: 213-237.

Singer, S., Puente, N., Sinito, A., Allmendinger, R., 1994. Estudio paleomagnético de secuencias Terciarias aflorantes al este del Salar de Antofalla, Puna Austral, Argentina. VII Congreso Geológico Chileno. Actas II: 1451-1455.

Sparks, R.S.J., Francis, P.W., Hamer, R.D., Pankhurst, R.J., O'Callaghan, L.O., Thorpe, R.S., Page, R.N., 1985. Ignimbrites of the Cerro Galán Caldera, NW Argentina. Journal of Volcanology and Geothermal Research, 24: 205-248.

Trumbull, R.B., Riller, U., Oncken, O., Scheuber, E., Munier, K., Hongn, F., 2006. The time-space distribution of Cenozoic arc volcanism in the Central Andes: a new date compilation and some tectonic implications. In: Oncken, O. et al. (eds) The Andes – Active Subduction Orogeny. Frontiers in Earth Sciences, 1. Springer-Verlag, Berlin, Heidelberg, New York, p. 29-43.

Voss, R., 2002. Cenozoic stratigraphy of the southern Salar de Antofalla Region, Northwestern Argentina. Revista Geológica de Chile 29: 167-189.

Whitman, D., Isacks, B.L., Chalelain, J.L., Chiu, J.M., Perez, A., 1992. Attenuation of high-frequency seismic waves beneath the Central Andean Plateau. Journal of Geophysical Research, 97: 19929-19947.

Whitman, D., Isacks, B.L., Kay, S.M., 1996. Lithospheric structure and along-strike segmentation of the Central Andean Plateau: seismic Q, magmatism, flexure, topography and tectonics. Tectonophysics, 259: 29-40.

Woelbern, I., Heit, B., Yuan, X., Asch, G., Kind, R., 2006. Crustal and upper mantle structures beneath the Central Andes at 21°S and 25.5°S derived from receiver functions. European Geosciences Union, Geophysical Research Abstracts, 8: 03709.

Figure captions

Figure 1. Sketch map showing the location of the study area (box) with respect to the Cenozoic magmatic arc (shaded). The main arc (Western Cordillera) is crossed by a number of NW-SE transverse lineament zones (simplified from Salfity, 1985), along which Cenozoic volcanism steps to the east.

Figure 2. Simplified geologic map of the southern Puna area, modified from Schnurr et al. (2006), showing the location of all dated samples and the trend of the Archibarca and Culampaja Lineaments from Fig. 1.

Figure 3. Whole-rock composition of the dated samples in the K_2O vs. SiO_2 (a) and TAS (b) classification diagrams, with field divisions from Middlemost (1980) and Le Maitre et al. (1989), respectively. For sources of compositional data see Table 2.

Figure 4. Ar release spectra and reverse isochrons from three samples from this study to illustrate typical degassing behavior during laser step-heating experiments, see text. Plateau-defining steps on the Ar release spectra are white, non-plateau steps are shaded.

Figure 5. Ar release spectra for all samples of this study not shown in Fig. 4. See text and appendix for discussion of plateau, total-gas and isochron ages.

Figure 6. Comparison of satellite images of dated volcanic features from this study to illustrate the difficulty of judging relative ages of volcanic features from remote-sensing data in high, arid regions like the Southern Puna plateau (images from Google Earth, ©2005Google, ©2007TerraMetrics).

Figure 7. Frequency – age histogram of mafic back-arc volcanism from 10 to 0 Ma (data from this study and Table 1 are stacked). Arrows indicate the main eruptions of ignimbrite from Cerro Galán caldera (Sparks et al., 1985). Also shown for comparison is the volcanic activity in the main arc for the same time period, based on the compilation in Trumbull et al. (2006), with geographic limits 25-27°S and 68- 69°W, and excluding ignimbrites (144 dated centers).

Figure 8. Sketch map of the study area showing the spatial distibution of dated back-arc ages based on new ^{40}Ar-^{39}Ar geochronology and our compilation of literature data in Table 1.

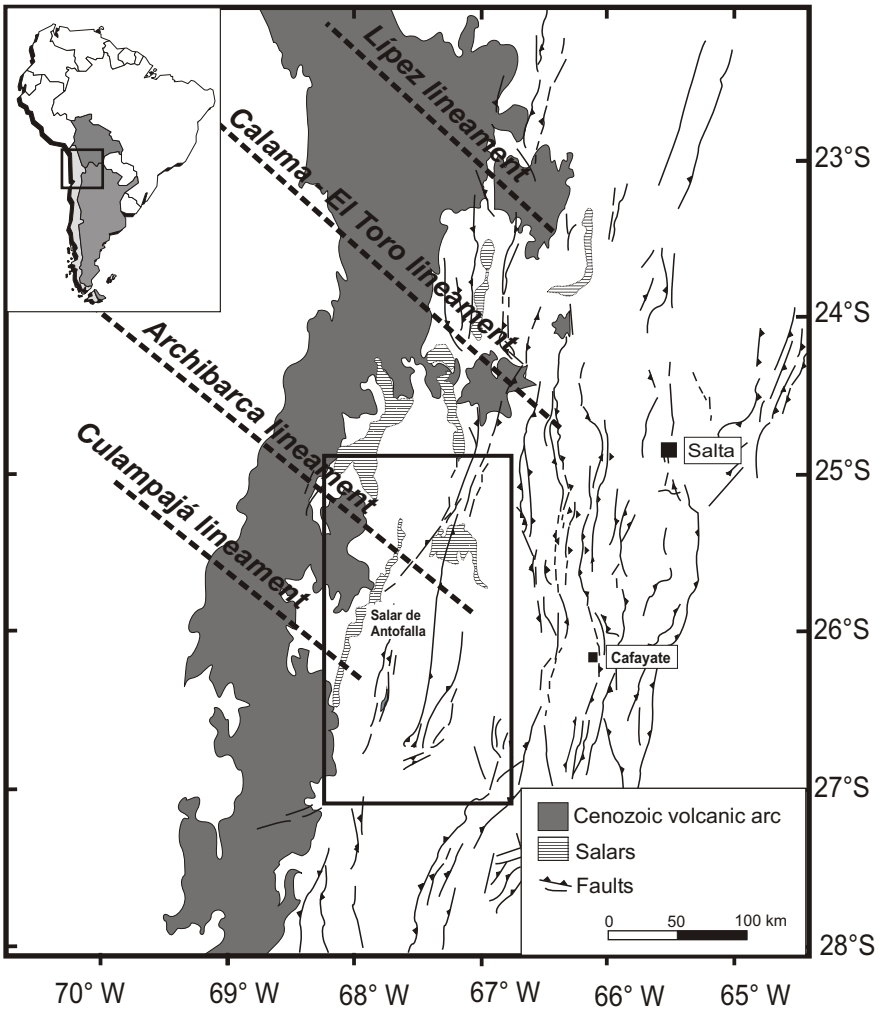

Risse et al. Fig. 1

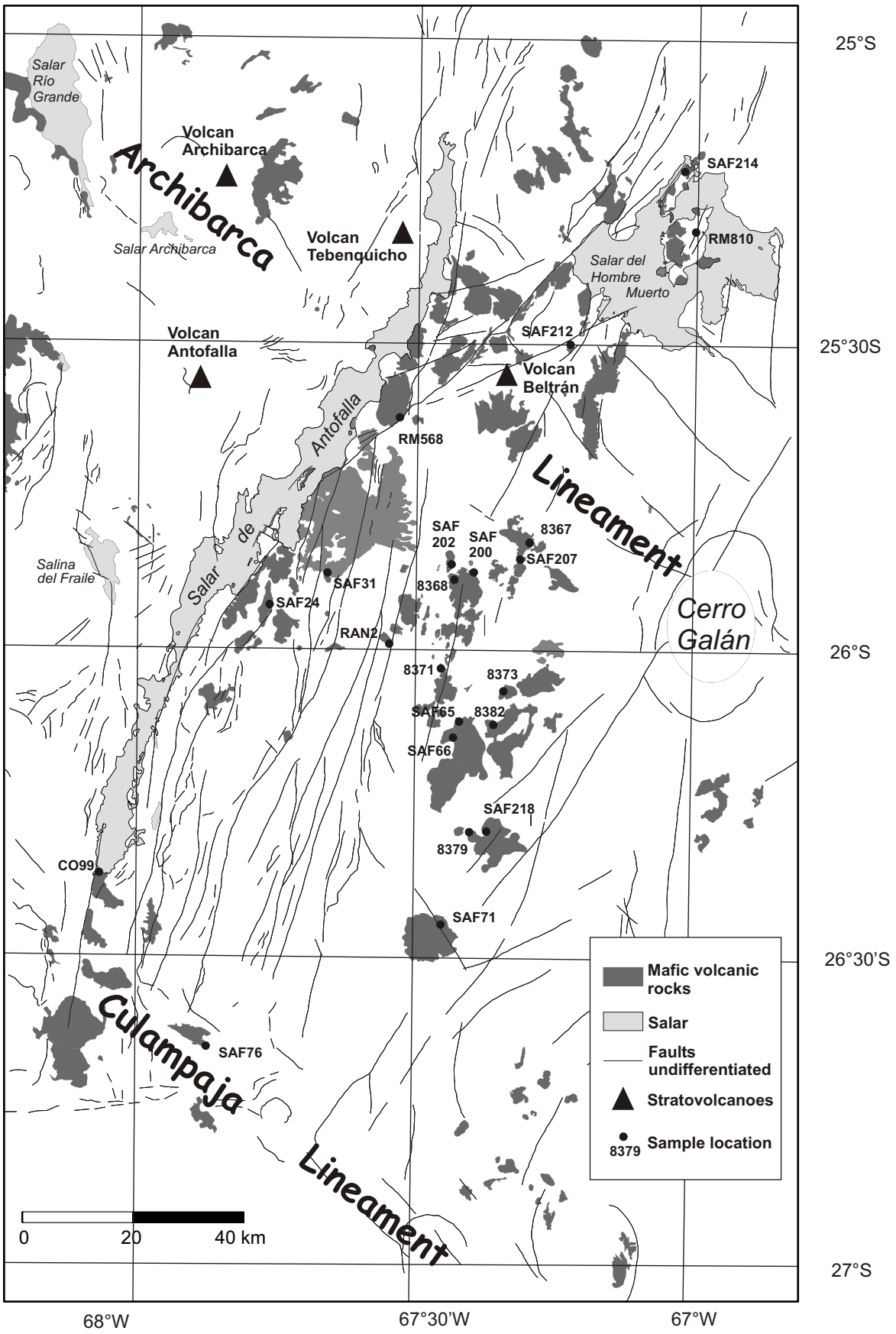

Risse et al. Fig. 2

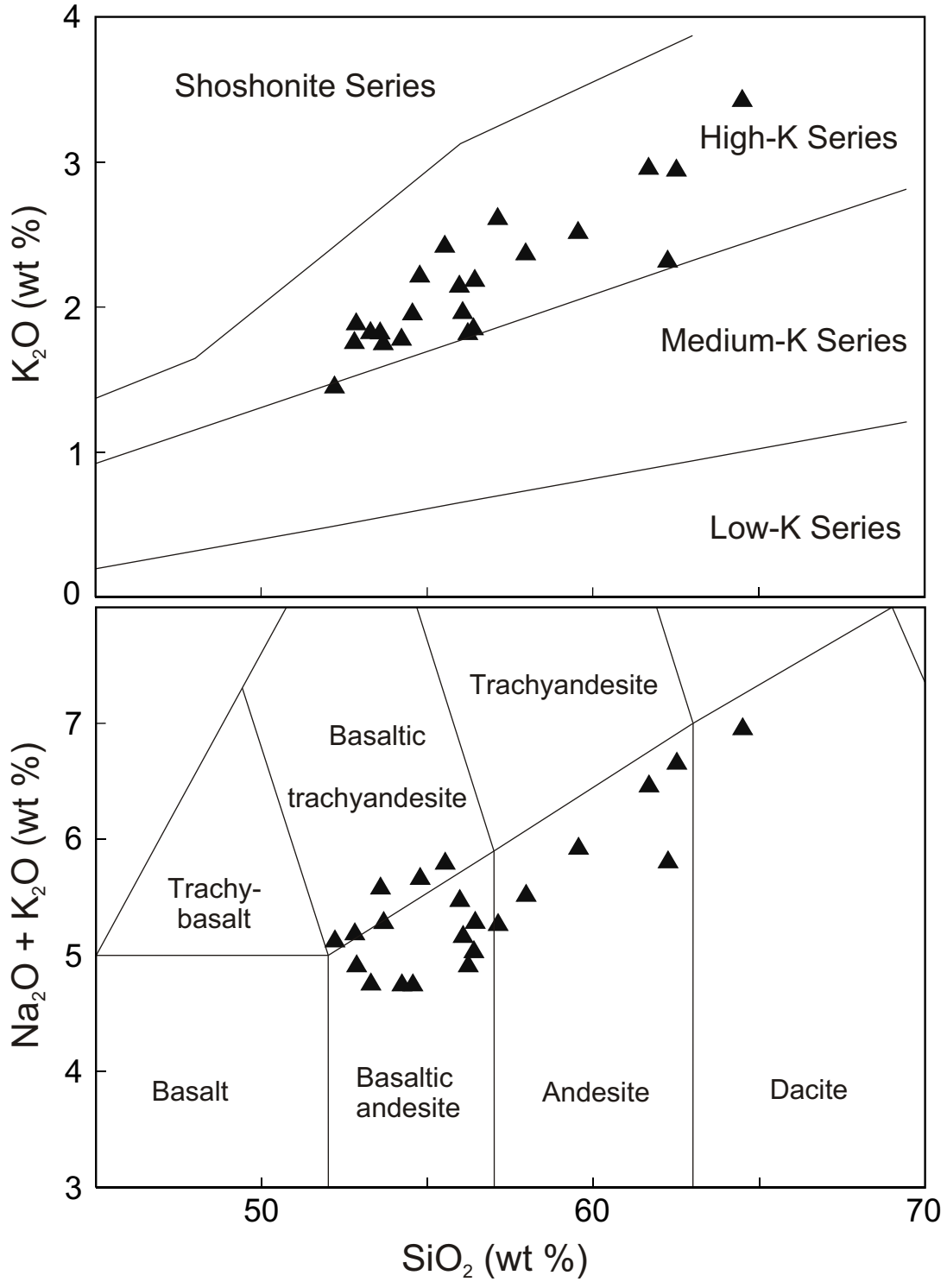

Risse et al., Fig. 3

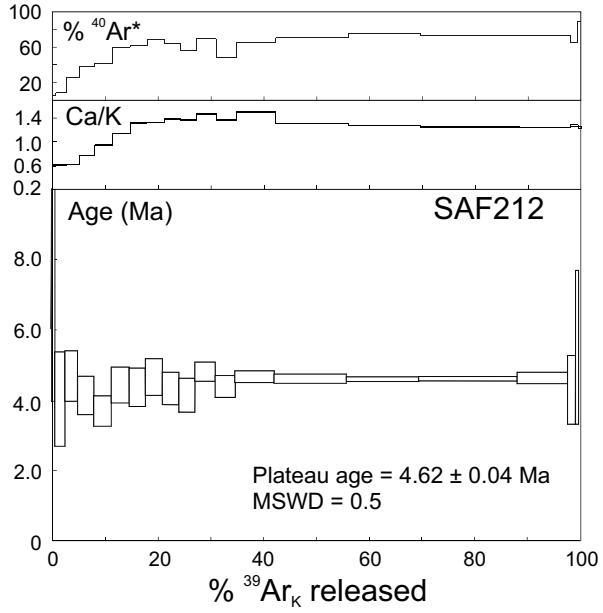

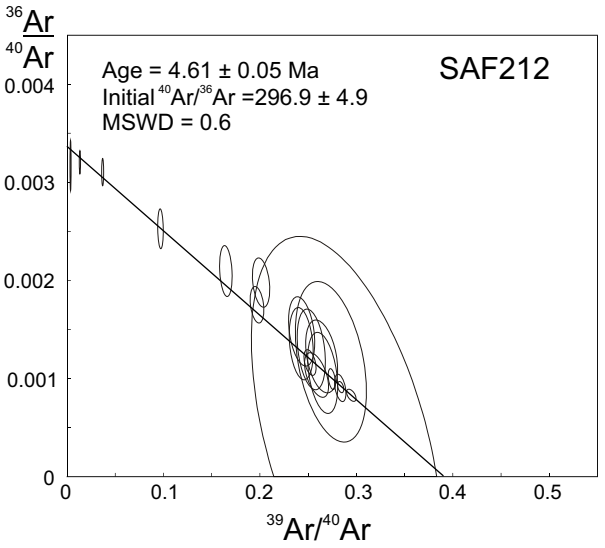

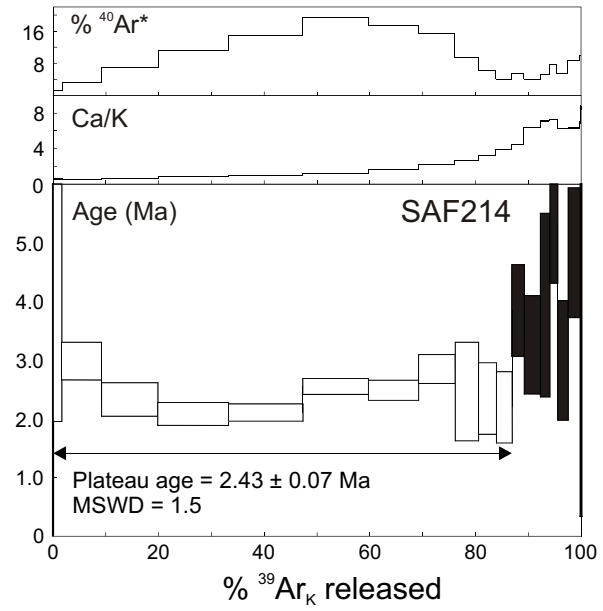

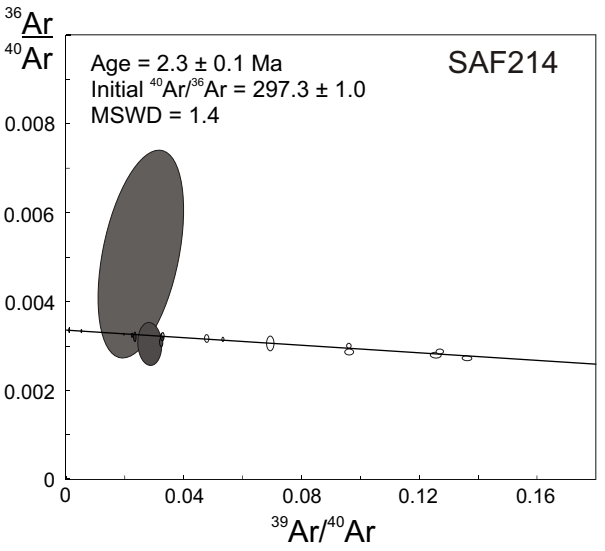

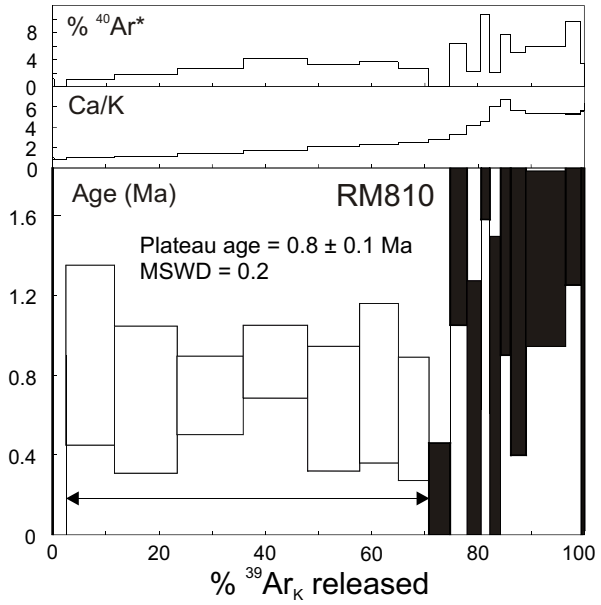

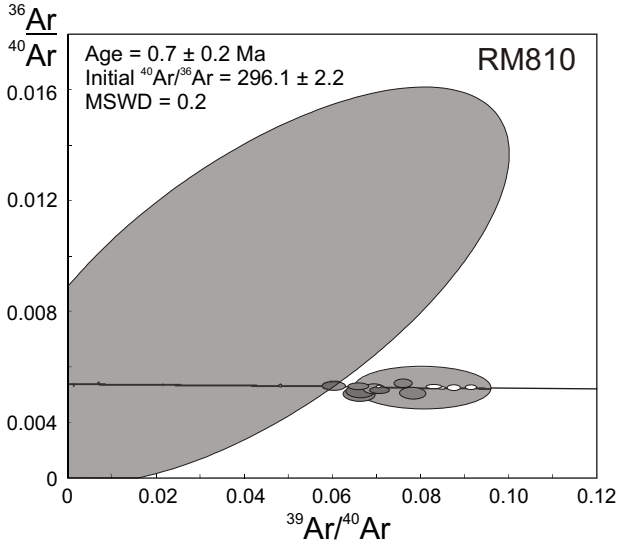

Risse et al., Fig. 4

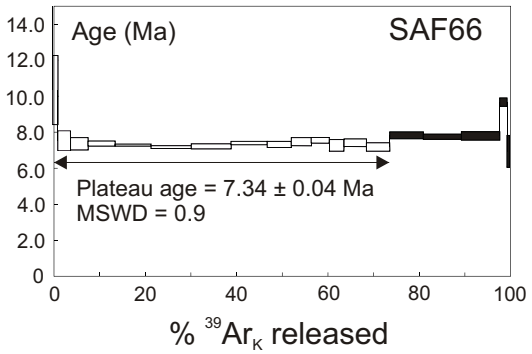

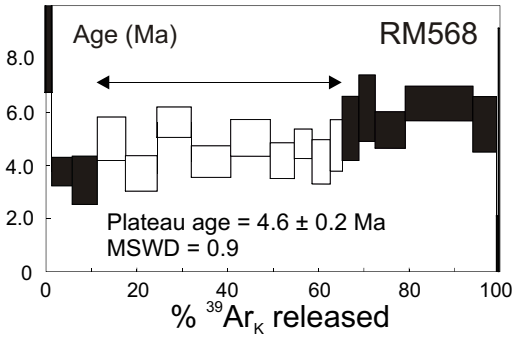

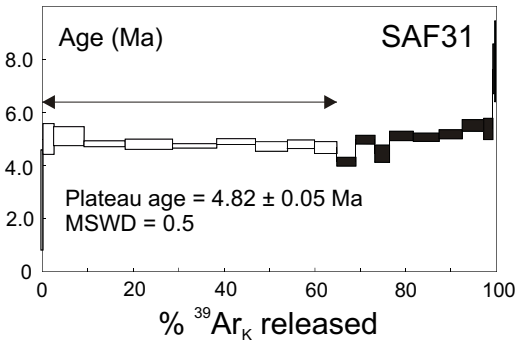

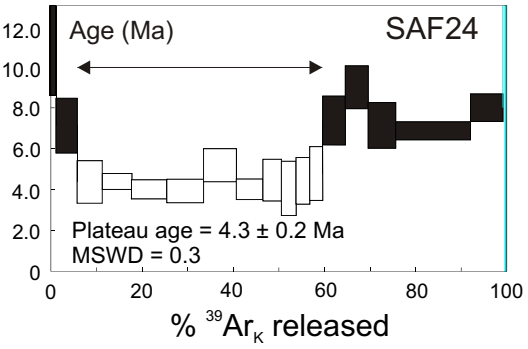

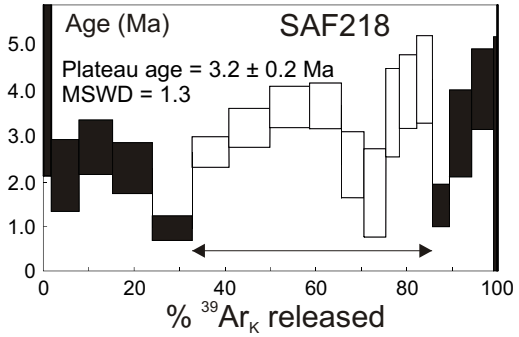

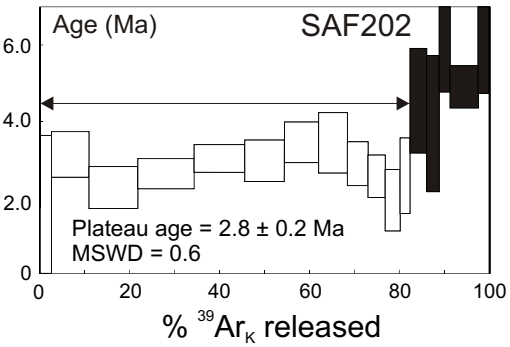

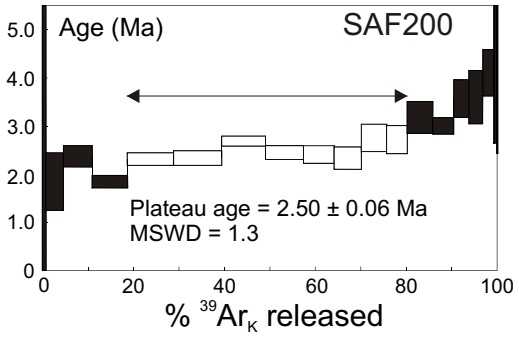

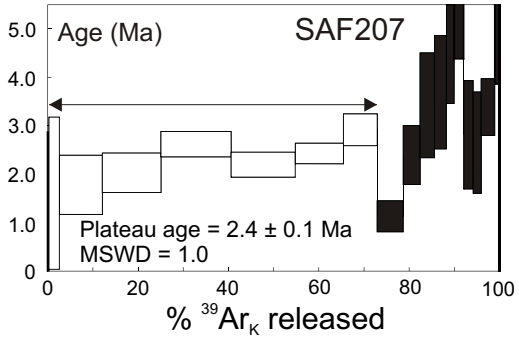

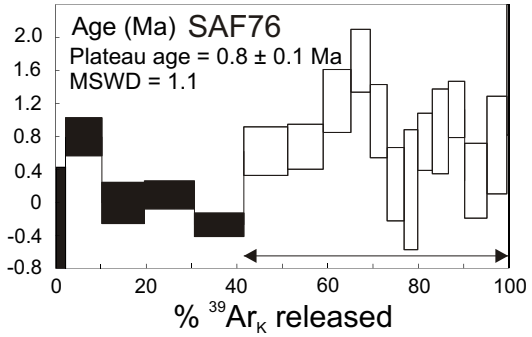

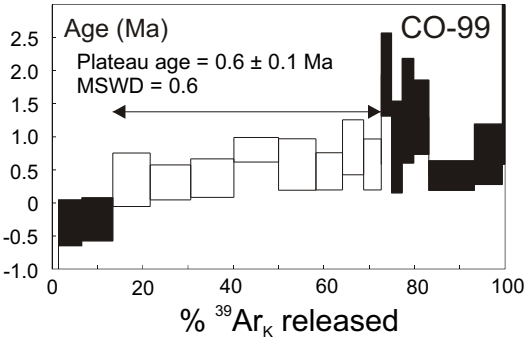

Risse et al., Fig. 5

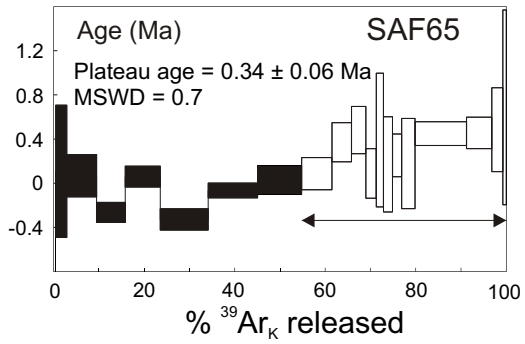

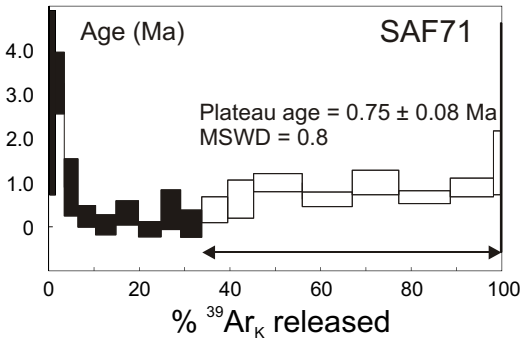

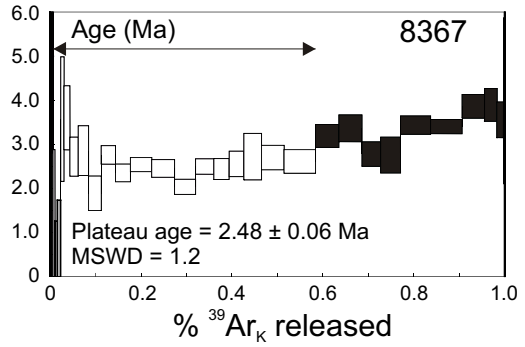

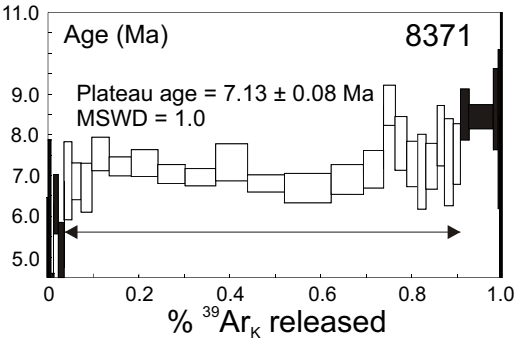

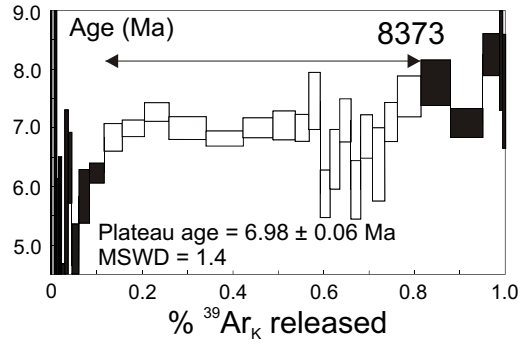

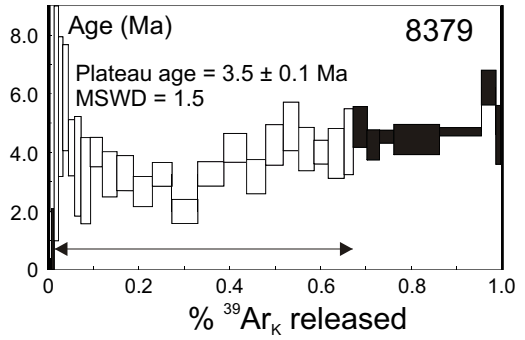

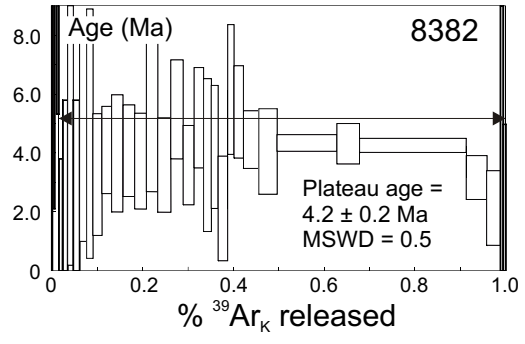

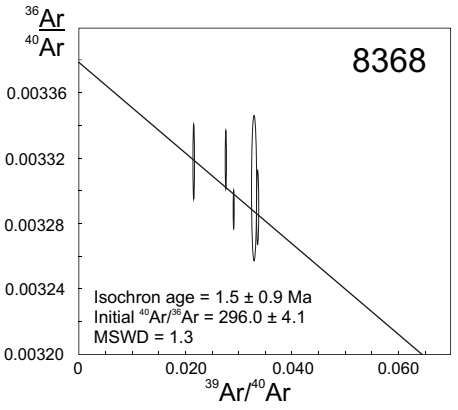

Risse et al., Fig. 5 (continued)

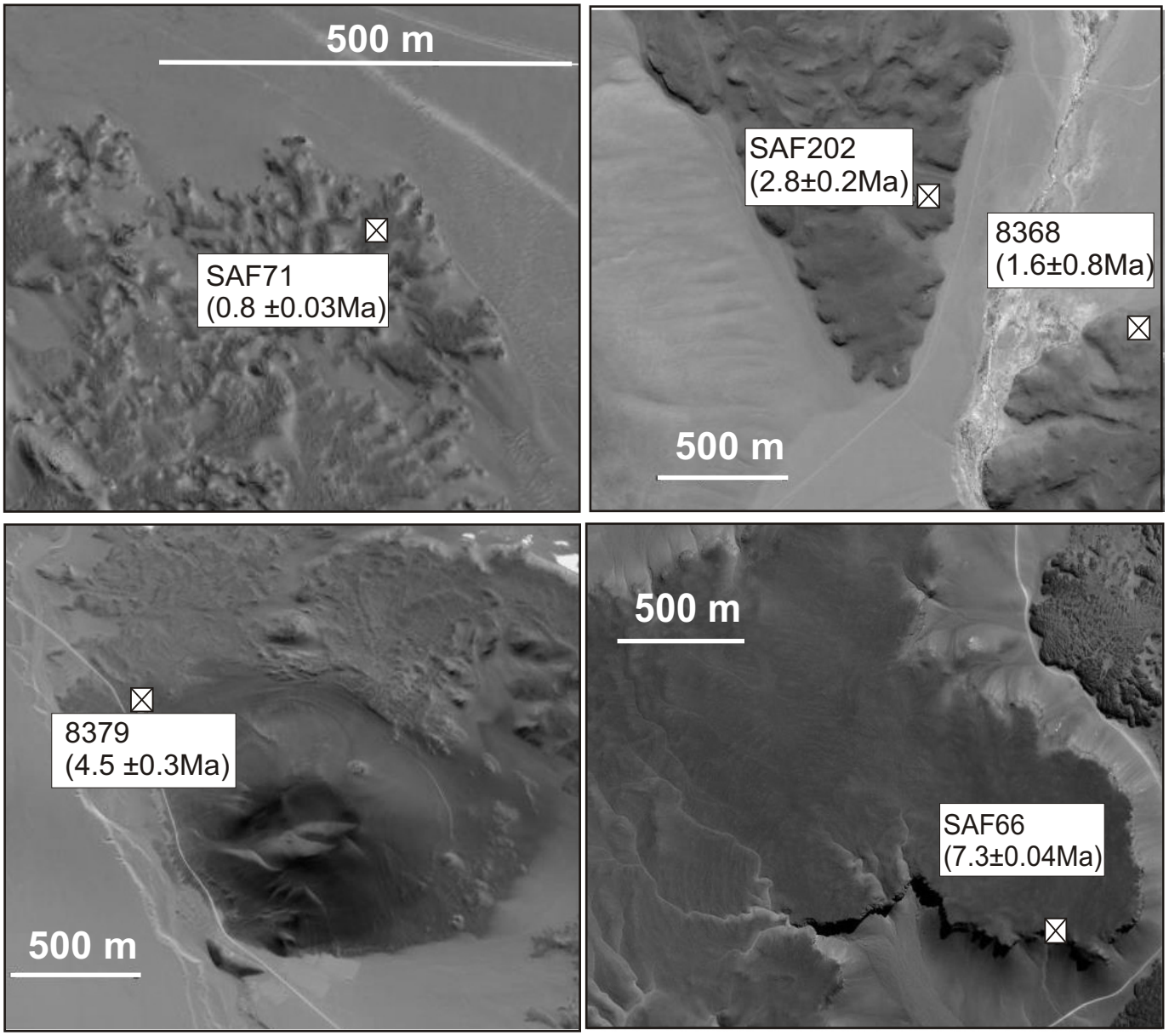

Risse et al. Fig. 6

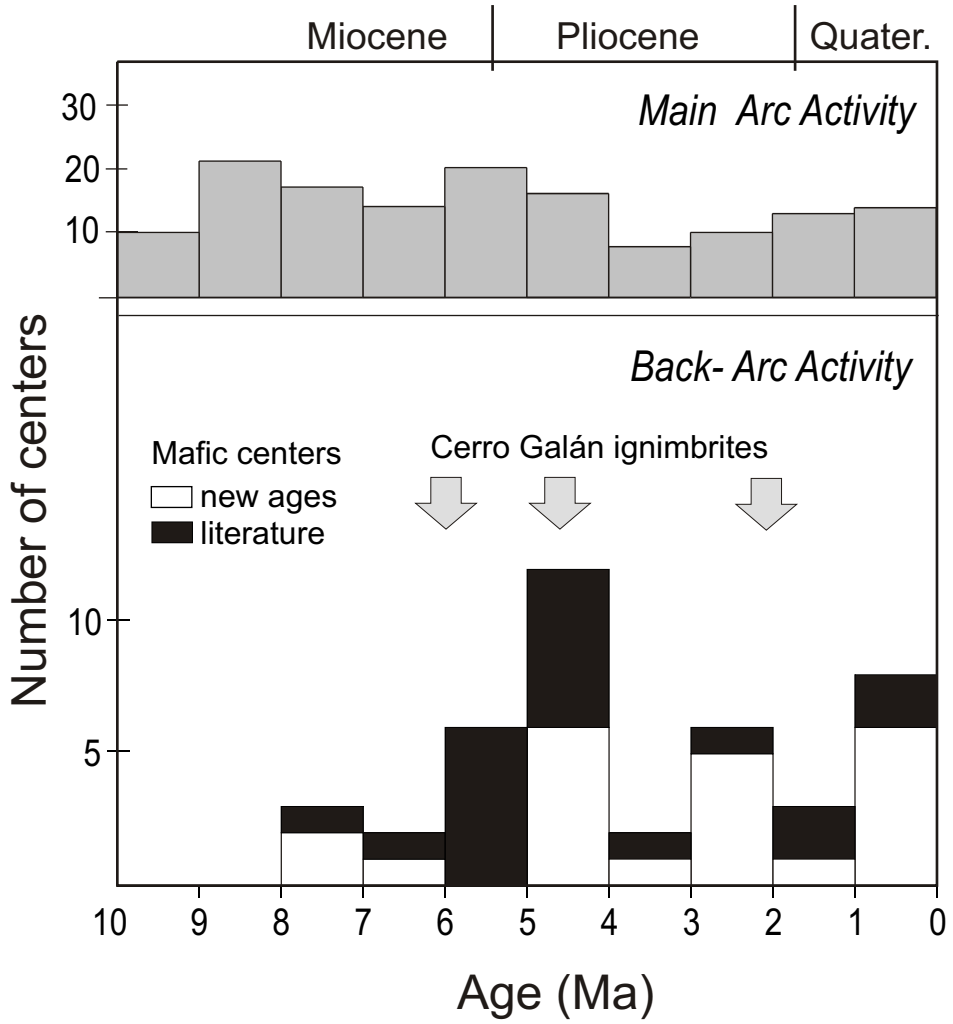

Risse et al. Fig. 7

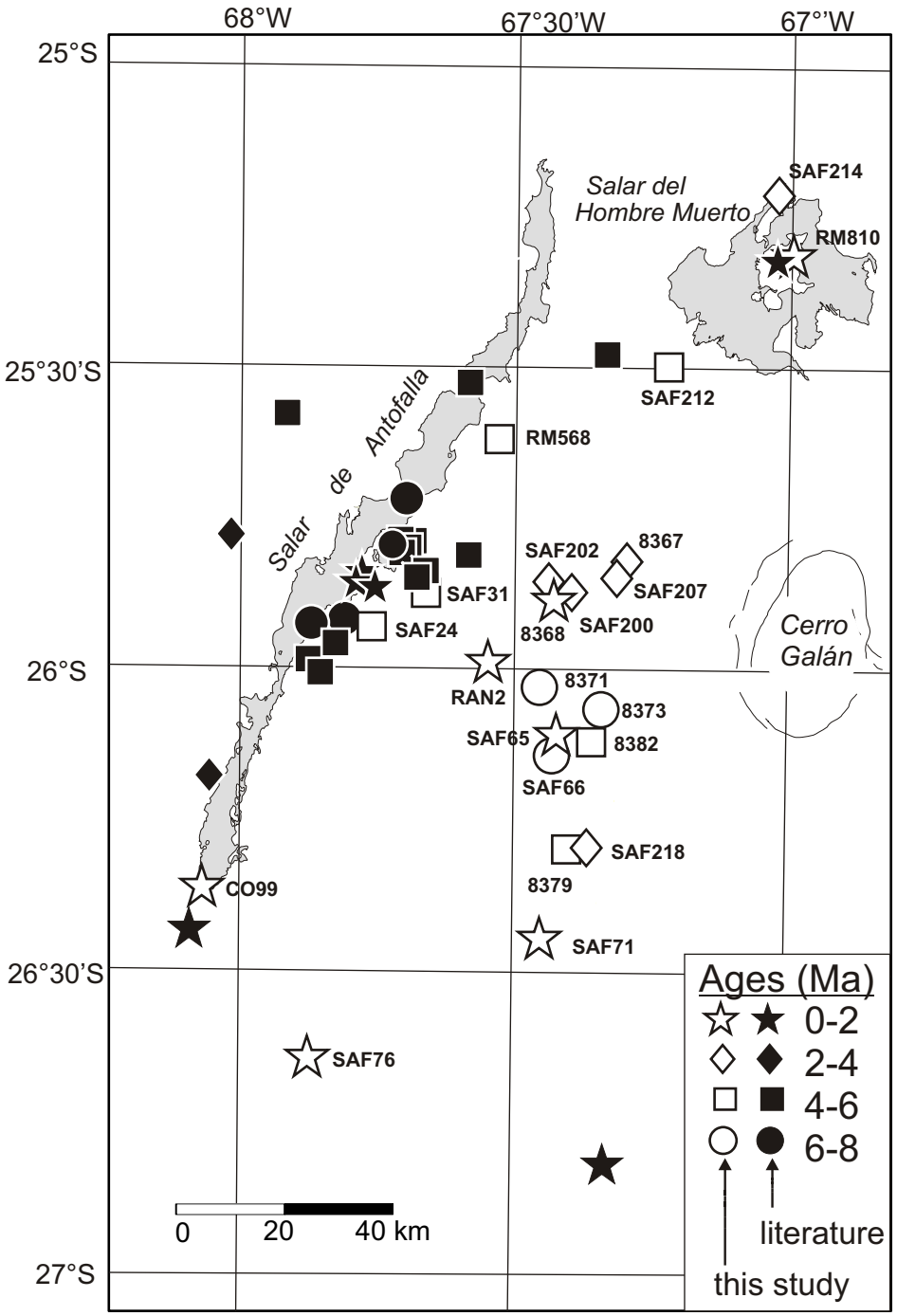

Risse et al. Fig. 8

Table 1. Compilation of published age data for back-arc volcanic centers in the southern Puna.

Rock type	Latitude	W- longitude	Age (Ma ± 1σ)	Method	Reference
B-A	26.408°S	68.079°W	0.2 ±0.09	Ar-Ar (matrix)	Kraemer et al. (1999)
B-A	25.992°S	67.867°W	4.6 ± 0.2	K-Ar (wr)	Kraemer et al. (1999)
B-A	25.812°S	67.585°W	4.68 ± 0.08	Ar-Ar (glass)	Kraemer et al. (1999)
BA	25.930°S	67.822°W	5.2 ± 0.3	K-Ar (wr)	Kraemer et al. (1999)
A	25.738°S	67.709°W	7 ± 0.3	K-Ar (wr)	Kraemer et al. (1999)
B-A	25.20°S	67.10°W	0.75 ± 0.03	K-Ar (wr)	Alonso et al. (1984)
B-A	26.80°S	67.40°W	1.3 ± 0.6	Ar-Ar (wr)	Marrett et al. (1994)
B-A	25.8°S	67.8°W	1.5 ± 0.4	K-Ar	Kay et al. (1997)
B-A	25.8°S	67.7°W	4.97 ± 0.07	Ar-Ar (matrix+plag)	Marrett et al. (1994)
B-A	25.8°S	67.7°W	5.03 ± 0.08	Ar-Ar (matrix+plag)	Marrett et al. (1994)
A	25.8°S	67.7°W	4.3 ± 0.5	Ar-Ar (matrix)	Marrett et al. (1994)
B-A	25.8°S	67.7°W	6.64 ± 0.07	Ar-Ar (matrix+plag)	Marrett et al. (1994)
B-A	25.8°S	67.7°W	4.9 ± 0.2	Ar-Ar	Marrett et al. (1994)
B	25.6°S	68.4°W	2 ± 1	K-Ar	Coira and Pezzutti (1976)
A	26.181°S	68.038°W	3.61 ± 0.02	Ar-Ar (Plag)	Voss (2002)
A	25.464°S	67.341°W	5.3 ± 0.3	K-Ar (wr)	Voss (2002)
B-A	25.58°S	67.92°W	4.8 ± 0.3	K-Ar (Bt)	Coira et al. (1993)
A	25.529°S	67.588°W	4.8 ± 0.5	Ar-Ar (Plag)	Adelmann (2001)
B	25.83°S	67.67°W	4.97 ± 0.07	?	Singer et al. (1994)
A	25.83°S	67.67°W	5.3 ± 0.8	?	Singer et al. (1994)
BA	26.032°S	67.863°W	5.6 ± 0.3	K-Ar (wr)	Adelmann (2001)

Rock type abbreviations: D- dacite, A- andesite, B - basalt, B-A basaltic andesite

Table 2. Location, description and preferred age of samples dated in this study.

Sample	latitude	longitude	Type[1]	Phenocrysts[2]	Matrix phases	Glass[3]	Age[4]	Comp. data[5]
SAF24*	25.93°S	67.76°W	B-TA	Ol	Cpx±Ol+Plag+Ox	< 5	4.3	2
SAF31	25.87°S	67.67°W	A	Ol+Cpx±Bt	Plag+Ox	20-25	4.8	3
SAF65	26.14°S	67.44°W	B-TA	Ol	Cpx+Plag+Ox	25-40	0.3	3
SAF66	26.130°S	67.428°W	A	Ol	Cpx+Plag+Ox	0	7.3	3
SAF71	26.471°S	67.416°W	B-TA	±Cpx	Ol+Cpx+Plag+Ox	0	0.8	3
SAF76	26.65°S	67.87°W	B-TA	Ol+Cpx	Cpx+Plag	0	0.8	3
SAF200	25.872°S	67.393°W	A	Ol+Cpx	Cpx+Plag+Ox	20-25	2.5	5
SAF202	25.870°S	67.436°W	B-A	Ol+Cpx	Cpx+Plag+Ox	15-20	2.8	5
SAF207	25.853°S	67.310°W	A	Ol	Plag+Cpx+Ox	30-40	2.4	5
SAF212	25.508°S	67.029°W	A	Cpx+Hbl±Plag	Plag	10	4.6	5
SAF214	26.306°S	67.390°W	B-A	Ol	Plag+Cpx±Ol+Ox	30	2.4	5
SAF218	26.306°S	67.390°W	B-A	Ol	Cpx+Plag	5	3.2	5
RAN2	25.992°S	67.543	B-A	Ol	Plag+Cpx±Ol+Ox	40	<0.1	5
CO-99	26.372°S	68.071°W	B-TA	Ol±Cpx	Cpx+Plag	0	0.6	3
RM568	25.62°S	67.54°W	B-A	Ol+Cpx	Plag+Ox±Ol±Cpx	< 5	4.6	1
RM810	25.53°S	67.00°W	B-A	Ol+Cpx	Plag±Cpx+Ox	50	0.8	1
8367	25.83°S	67.30°W	B-TA				2.5	4
8368	25.90°S	67.44°W	A				1.5	4
8371	26.03°S	67.46°W	A				7.1	4
8373	26.07°S	67.55°W	D				7.0	4
8379	26.30°S	67.41°W	B-A				4.5	4
8382	26.12°S	67.36°W	A				4.2	4

* SAF24 = SAF25 in Kay et al. (1999)

1: A- andesite, B-A basaltic andesite, B-TA basaltic trachyandesite, T-A trachyandesite, D-dacite

2: Ol-olivine, Cpx-clinopyroxene, Bt-biotite, Hbl-hornblende, Plag-plagioclase, Ox – Fe-Ti Oxide

3: Volume percentage of glass in the matrix, estimated and not point-counted

4: Preferred age from ^{40}Ar-/^{39}Ar step-heating analysis, typical 1σ errors are 0.1 Ma, see Appendix

5: Reference for compositional data used in Figure 3: 1- Kay et al., 1994; 2- Kay et al., 1999; 3-Kay and Coira, unpubl. 4- van den Bogaard, unpublished; 5- Risse in prep.

Appendix. Summary of $^{40}Ar/^{39}Ar$ results for mafic volcanic rocks of the southern Puna plateau

Sample	Location	Plateau age					Isochron age							Integrated age			XRF data		
		age (Ma)	1 σ	^{39}Ar (%)	steps[1]	MSWD	age (Ma)	1 σ	$^{40}Ar/^{36}Ar$ intercept	1 σ	steps[1]	MSWD	prob. of fit [2]	age (Ma)	1 σ	K/Ca[3]	K_2O	CaO	K/Ca molar
SAF66	La Alumbrera older flow	**7.34**	**0.04**	73.7	14(20)	0.9	7.3	0.05	296.8	0.7	14(20)	0.7	0.77	7.64	0.05	0.81	2.3	4.93	0.56
RM568	Vegas Colorado	4.9	0.2	88.4	16(20)	1.2	4.9	1.4	294.9	3.5	9(20)	1.0	0.41	5.10	0.2	0.35	1.81	6.37	0.34
	Salar de Antofalla	**4.6**	**0.2**	54.0	9(20)	0.9													
SAF31	N Cerro Chato Peninsula Camp 2	**4.82**	**0.05**	65.1	10(20)	0.5	4.9	0.1	295.2	0.9	10(20)	0.5	0.86	4.92	0.05	0.82	2.93	5.26	0.66
SAF212	NE Lago Caro	**4.62**	**0.04**	100.0	20(20)	0.5	4.61	0.05	296.9	4.9	20(20)	0.6	0.92	4.58	0.07	0.80	2.90	4.89	0.71
SAF24	DIABLO Peninsula	**4.3**	**0.2**	53.8	10(20)	0.3	3.7	1.4	297.2	3.8	10(20)	0.3	0.96	6.1	0.2	0.29	1.73	8.22	0.25
SAF218	El Jote	**3.2**	**0.2**	52.9	9(20)	1.3	-3.5	3.4	324.0	14.0	9(20)	0.8	0.58	2.9	0.2	0.35	1.83	8.40	0.26
							1.6	0.8	299.2	3.2	20(20)	3.4	0.00						
SAF202	Los Nacimientos	2.9	0.2	88.8	15(20)	0.7	2.8	0.3	295.6	1.3	13(20)	0.7	0.76	3.3	0.2	0.35	1.91	7.52	0.30
		2.8	**0.2**	82.3	13(20)	0.6													
SAF200	Los Nacimientos	**2.5**	**0.06**	61.5	8(20)	1.3	2.5	0.1	293.7	1.3	13(20)	2.3	0.01	2.61	0.06	0.52	2.31	6.26	0.44
SAF214	N Hombre Muerto,	2.44	0.07	92.1	13(20)	1.6	2.3	0.1	297.3	1.0	11(20)	1.4	0.18	2.6	0.1	0.50	1.76	6.97	0.30
	Tincalayu	**2.43**	**0.07**	86.8	11(20)	1.5													
SAF207	E Cerro Chinina	**2.4**	**0.1**	72.9	8(20)	1.0	2.8	0.2	293.2	1.5	8(20)	0.7	0.62	2.5	0.1	0.55	2.54	6.18	0.49
SAF76	Cuerros Purulla	**0.8**	**0.1**	58.5	14(20)	1.1	0.3	0.2	296.2	1.8	20(20)	3.5	0.00	0.46	0.09	0.51	2.37	6.92	0.41
RM810	Farallon Catal ,	0.79	0.09	100.0	20(20)	1.5	0.7	0.2	296.1	2.2	7(20)	0.2	0.96	0.8	0.1	0.39	1.94	7.36	0.31
	Salar de Hombre Muerto	**0.8**	**0.1**	68.1	7(20)	0.2													
CO99	S Salar de Antofalla	0.62	0.09	87.0	16(20)	0.9	0.8	0.1	291.1	1.2	20(20)	1.0	0.50	0.5	0.1	0.30	1.77	7.91	0.27
		0.6	**0.1**	59.3	8(20)	0.6													
SAF65	La Laguna	0.34	0.06	45.2	12(20)	0.7	-0.1	0.2	298.7	3.3	20(20)	3.5	0.00	0.09	0.04	0.42	1.73	7.48	0.28
SAF71	Carachi Pampa	**0.75**	**0.08**	66.3	9(20)	0.8	-0.2	0.3	301.3	2.0	20(20)	1.9	0.01	0.73	0.08	0.30	1.44	7.7	0.22
RAN2	La Falda	0.03	0.04	100.0	20(20)	1.0	0.01	0.06	296.4	0.9	20(20)	1.0	0.43	0.04	0.05	0.33	1.74	7.31	0.28
8379	S Antofagasta valley	3.5	0.1	65.8	21(36)	1.5	1.8	0.6	299.0	1.2	21(36)	1.1	0.33	4.0	0.1	0.58	2.83	4.69	0.72
							4.5	**0.3**	294.9	0.6	36(36)	3.1	0.00						
8382	E slope Antofagasta valley	**4.2**	**0.2**	99.0	31(35)	0.5	4.2	0.2	296.4	2.0	31(35)	0.5	0.99	4.1	0.2	1.22	2.52	5.74	0.52
8373	E Antofagasta valley	**6.98**	**0.06**	69.8	17(36)	1.4	7.0	0.2	295.1	1.7	17(36)	1.5	0.09	6.8	0.08	2.29	3.37	4.2	0.96
8368[4]	W Antofagasta valley						**1.5**	**0.8**	296.0	4.1	n=5	1.3	0.29	1.5	0.1	0.84	2.17	6.58	0.39
8367	N Cerro Merihuaca	**2.48**	**0.06**	58.4	24(37)	1.2	2.43	0.09	295.9	0.5	24(37)	1.2	0.22	2.88	0.06	0.83	2.14	3.33	0.77
8371	Road to Antofalla	**7.13**	**0.08**	87.2	21(35)	1.0	6.9	0.3	296.3	1.1	21(35)	1.0	0.38	7.13	0.09	0.97	2.19	8.4	0.31

Preferred ages are in bold type.

1 - Steps used to define the plateau or isochron ages, with total number of heating steps in parenthesis. Where two values are given, the first refers to the plateau identified by Isoplot 3.00 (Ludwig, 2003), and the second to a more restricted plateau excluding high-T steps (see text). Steps for isochron regression are as indicated; for SAF200, 5 low-T steps were added to improve precision.

2 - Probability of fit after Ludwig (2003). Values < 0.15 indicate that scatter around the regression line is due to analytical errors only.

3 - K/Ca ratios calculated from recombined totals of $^{39}Ar_K$ and $^{37}Ar_{Ca}$.

4 - The sample was analysed by total fusion of 5 fragments.